Number size distribution of aerosol particles and new particle formation events in tropical and subtropical Pacific Oceans

doi: 10.1016/j.atmosenv.2016.07.055

Atmospheric Environment 142 (2016) 324–339

Contents lists available at ScienceDirect

Atmospheric Environment

journal homepage: www.elsevier.com/locate/atmosenv

Number–size distribution of aerosol particles and new particle formation events in tropical and subtropical Pacific Oceans

S. Ueda [a, *], K. Miura [a], R. Kawata [b], H. Furutani [b, 1], M. Uematsu [b], Y. Omori [c, 2], H. Tanimoto [c]

[a] Faculty of Science, Tokyo University of Science, Tokyo, Japan
[b] Atmosphere and Ocean Research Institute, The University of Tokyo, Chiba, Japan
[c] National Institute for Environmental Studies, Tsukuba, Ibaraki, Japan

HIGHLIGHTS

- Aerosol number–size distributions were observed over the North and South Pacific.
- Distributions over respective areas were parameterized using lognormal fitting.
- Bimodal distributions of larger peaks were observed over the eastern equator.
- New particle formation occurred often at eastern South Pacific mid-latitudes.

ARTICLE INFO

Article history:
Received 23 April 2016
Received in revised form
14 July 2016
Accepted 29 July 2016
Available online 31 July 2016

Keywords:
Atmospheric aerosols
Number–size distribution
Marine boundary layer
New particle formation
Dimethyl sulfide

ABSTRACT

Number–size distributions of aerosol particles with diameters of 10–500 nm in the marine boundary layer were observed continually onboard the *R/V Hakuho Maru* over the equatorial and subtropical North Pacific and South Pacific during December 2011–March 2012. Number–size distributions over each area were parameterized using a sum of up to three lognormal functions. Bi-modal size distributions with peak diameters at 30–80 nm (Aitken mode) and 100–200 nm (accumulation mode) were observed frequently. Larger peak diameters of Aitken and accumulation modes were observed over the eastern equator, where 5-day backward trajectories showed that the air masses had derived from high-chlorophyll oceanic regions without precipitation. Smaller peak diameters and low concentrations were often observed over the North Pacific. The trajectories show that such air mass originated from oceanic regions with less chlorophyll, exhibiting high precipitation frequency. New particle formation (NPF) events have often been observed over the mid-latitude eastern South Pacific with a low condensation sink (CS) and some dimethyl sulfide, although none was observed over the equator, where CS was higher. The lesser CS condition at NPF events was mostly correlated with local precipitation or precipitation along the trajectories within 1 day. These results suggest that differences of the number–size distribution and occasions of NPF events among sea areas most closely accord with precipitation along the trajectories.

1. Introduction

Aerosol particles play an important role in Earth's climate systems by directly scattering and absorbing solar radiation and by acting indirectly as cloud condensation nuclei (CCN) (Twomey, 1977). The particles affect Earth's radiation budget and therefore affect its climate. Stratocumulus clouds that extend over large ocean regions can influence the aerosol size distribution through in-cloud processing and wet scavenging and by the influence of the albedo of aerosols and clouds, affecting solar energy input into the

* Corresponding author. Graduate School of Environmental Studies, Nagoya University, Nagoya, Japan.
E-mail address: ueda-s@stelab.nagoya-u.ac.jp (S. Ueda).
[1] Now at the Center for Scientific Instrument Renovation and Manufacturing Support, Osaka University, Osaka, Japan.
[2] Now at the Faculty of Life and Environmental Sciences, University of Tsukuba, Tsukuba, Japan.

http://dx.doi.org/10.1016/j.atmosenv.2016.07.055

Earth atmosphere system. One determining factor of the cloud albedo is the cloud droplet concentration, which is controlled to a great degree by the updraft velocity at the cloud base and the number concentration of aerosols that can become CCN (Seinfeld and Pandis, 2006; Twomey and Warner, 1967): a particle's size and chemical composition affect its ability to act as CCN (Köhler, 1936). Results of several field studies conducted in remote areas suggest that the particle size, and therefore the number–size distribution, strongly affects the total CCN concentration (Dusek et al., 2006; Fitzgerald, 1973; Junge and McLaren, 1971). The number–size distribution of atmospheric aerosol particles, particularly in the submicrometer size range, is indispensable for the simulation of direct scattering and cloud formation from aerosols. Nevertheless, size distributions vary greatly with variation of the number concentration for each size mode in the range of about three or for order according to time and space. Such fundamental properties of aerosols having variable size distribution are difficult to simulate accurately in the model because of a lack of understanding of processes and factors that affect the actual number–size distribution of atmospheric aerosols.

Although actual atmospheric number–size distributions vary greatly, the number–size distribution of atmospheric aerosols can be expressed as a continuous and multimodal distribution (Whitby, 1978). For the approximation of a number–size distribution of submicron aerosol particles, three typical lognormal modes called accumulation, Aitken, and nucleation modes have often been used (Kulmala et al., 2004; Raes et al., 2000). Each mode is generally regarded as reflecting a different part of the growth process: nucleation and condensation of semi-volatile vapors to particles constitutes the nucleation mode; then the nucleation mode evolves continuously to Aitken mode by condensation and coagulation; the accumulation mode particles are generally regarded as formed from Aitken mode particles, mainly by in-cloud processes (Fuchs, 1964; Hoppel et al., 1986; Husar and Whitby, 1973; Mamane and Gottlieb, 1989; Meng and Seinfeld, 1994; Ueda et al., 2014). Over remote seas, where precursors are less abundant, accumulation mode can be affected by primary sea salt emissions in addition to in-cloud processes (Clarke et al., 2006; Gong, 2003). Maritime aerosol particles over the Pacific Ocean have been studied by airplane observation (Clarke et al., 1998a, b; Roberts et al., 2006) and by ship observation (e.g. Andreae et al., 1995; Bates et al., 1998, 2002; Clarke and Porter, 1993; Clarke et al., 1987; Eleftheriadisa et al., 2006; Hoppel and Frick, 1990; Mochida et al., 2011; Pant et al., 2009; Raemdonck et al., 1986). Those observations have often revealed bimodal distributions that include Aitken mode and accumulation mode. The valley between the two modes has been attributed to in-cloud processing (Hoell et al., 2000; Hoppel et al., 1986, 1994a, 1994b; Mochida et al., 2011).

Natural marine aerosol particles comprise primary and secondary aerosol components (O'Dowd and Leeuw, 2007): the primary aerosols are produced by interaction of wind stress at the ocean surface and bubble-bursting process; the secondary aerosols are produced through gas-to-particle conversion processes of volatile marine biogenic matter. The sulfates are major compositions of sub-micrometer particles in the marine boundary layer (Fitzgerald, 1991). Some of the sulfuric acid is regarded as derived from the oxidation of dimethyl sulfide (DMS) emitted by marine phytoplankton (Charlson et al., 1987; Cox and Sandalls, 1974; Lovelock et al., 1972). According to ship experiments over the tropical South Atlantic conducted by Andreae et al. (1995), aerosol (CN and CCN) numbers, and non-sea-salt sulfate concentrations exhibited weak correlation with DMS concentration and flux. Nucleation and subsequent growth to Aitken mode particles in maritime air has been reported for coastal areas (Modini et al., 2009; Vaattovaara et al., 2006), suggesting that secondary aerosol formation occurs even in remote marine environments and that it affects the number–size distribution of marine aerosols. In eutrophic oceanic regions, marine biological activity and resultant marine biogenic matter emitted from the ocean to the atmosphere can affect the particle growth and the number–size distribution more strongly. Several reports have described observational evidence for particle nucleation in the marine boundary layer (MBL) along the coast of Washington state (Covert et al., 1992) and tropical areas of the Pacific Ocean (Clarke and Porter, 1993; Clarke et al., 1998a, 1999), but open-ocean cases and areas are few. Clarke et al. (1998a) conducted aircraft observations over the Pacific Ocean and observed a nucleation event during a 360-km-long near-surface flight, although the case was rare. The event occurred near the top of the MBL under highly scavenged MBL conditions with low surface area. They inferred that the newly observed particle formation event was related to the atmospheric oxidation of DMS emitted from marine biota and subsequent new particle formation under precipitation conditions.

The occurrence of new particle formation events is controlled not only by the precursor gaseous presence but also by pre-existing particle concentrations (Kulmala et al., 2001) because of the condensation of the precursor gaseous materials and coagulation of nucleated particles onto pre-existing particle surfaces. Actually, the events have often been found under low aerosol concentration conditions in remote areas (Nishita et al., 2008; Venzac et al., 2008). The precursor gaseous materials can affect the size distribution by new particle formation or growth of preexisting particles because of competing condensation of preexisting particle surfaces and in-cloud wet-aerosol aqueous chemistry. Therefore, their balance over marine areas might differ among areas depending on marine biogenic matter emissions, meteorological conditions related to aging, scavenging, and transportation processes.

Although many observations have been conducted over a broad ocean area as described above, the knowledge of aerosols over broad ocean areas will be insufficient. In some ocean areas such as the equator and southern east areas of Pacific Ocean, cases and periods of ship observation were few. Observational evidence of nucleation is especially limited. To observe the number–size distribution over a broad Pacific Ocean area, we conducted atmospheric observations onboard the R/V *Hakuho Maru* cruises during December 2011–March 2012. The courses of R/V *Hakuho Maru* cruises included oligotrophic oceanic regions in the south and north subtropical Pacific Ocean and eutrophic sea areas in the eastern tropical Pacific area. The main objective of this study was to ascertain the size distribution of aerosols over a broad marine area with regionally varying marine biological productivity and meteorological conditions, in addition to assessing their relation with new particle formation events.

2. Field observation and data analysis

2.1. Atmospheric observation

Aerosol observations were conducted over the Pacific Ocean on the R/V *Hakuho Maru* during the KH-11-10 and KH-12-1 cruises conducted 1 December 2011–7 March 2012. The ship's track is presented in Fig. 1. The KH-11-10 cruise started from Tokyo, Japan and reached Callao, Peru via Hawaii, USA and the mid-latitudes of the western South Pacific Ocean. The KH-12-1 (EqPOS: Equatorial Pacific Ocean and Stratospheric/Tropospheric Atmosphere Study) cruise started from Callao, Peru and reached Tokyo, Japan via the eastern equator and Hawaii, USA. The number–size distributions of dried aerosol particles were measured using a scanning mobility particle sizer (3034; TSI Inc.) for 10–500 nm and a laser particle counter (LPC, KC01D; Rion Co. Ltd.) for particle diameters greater

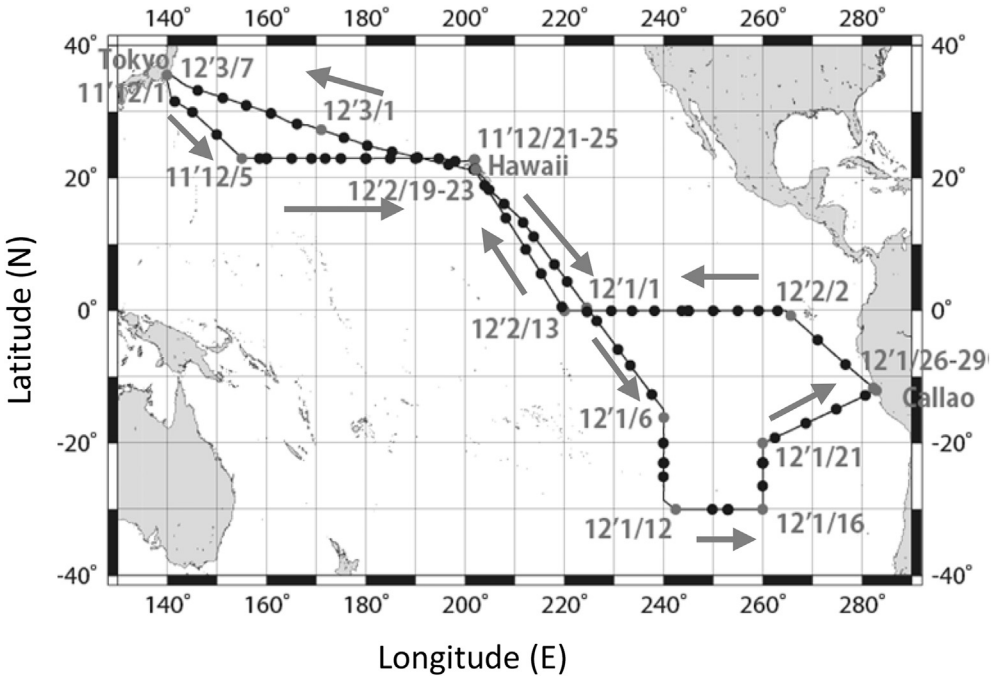

Fig. 1. Ship tracks of the KH-11-10 and KH-12-1 (EqPOS) cruises of the R/V *Hakuho Maru*.

than 0.3, 0.5, 1, 2, and 5 μm. These devices were placed in a cantina box installed in the foremost area of the compass deck (upper deck) of the ship to avoid ship exhaust contamination and particle loss in the long tube. The inlet was 0.5 m above the cantina. No wind interceptor exists around the inlet. The compass deck is approximately 13 m long, with 14 m height from the sea surface. The exhaust outlets of the kitchen and funnel are located respectively at distances of 15 m and 20 m behind the cantina. Particle number measurements were conducted with a 3 min cycle.

In addition to aerosols, carbon monoxide (CO) and ozone (O_3) were measured as trace gases. For both CO and O_3 measurements, atmospheric air was drawn from approximately 3 m above the roof of the wheel house through a ¼″ (6.4 mm) OD. It was then delivered to O_3 and CO instruments located inside the wheel house. The atmospheric CO gas concentration was measured using a non-dispersive CO analyzer (48C; Thermo) with CO-HC reactor-type zero gas generators (96; Thermo) for zero measurement. Atmospheric O_3 concentrations were monitored continuously during KH-11-10 and the EqPOS cruise using a UV absorption O_3 monitor (1150; Dyleck, Japan). To avoid water vapor condensation within the monitor, the sampled atmospheric air was dried with an electric air dryer (EC-95; Dyleck, Japan) before it was introduced into the monitor.

2.2. Analyses of aerosol number–size distributions

2.2.1. Data screening

To discuss background aerosol particles, we carefully examined some screening methods for ship self-emissions. Fig. 2a, b and c respectively portray examples of a number–size distribution before data screening, the total number concentrations of 10–500 nm particles ($N_{10\text{-}500}$), and relative wind direction and speed. Based on short-term variation of the total number, data showing the possibility of contamination from the ship exhaust were eliminated from the following analyses. Number concentrations calculated with data obtained when the ship exhaust was blown by wind from the rear of the ship showed particularly high values that varied dramatically in a short time. To eliminate data showing ship exhaust contamination, data were collected according to the temporal variation of the total number concentrations of 10–500 nm particles ($N_{10\text{-}500}$). We applied restrictions to the obtained data and eliminated suspect data that did not conform to the following: (1) standard deviation value of $N_{10\text{-}500}$ during 21 min ((3 min) data ± tree (9 min) data) less than 10% of the median value of $N_{10\text{-}500}$; (2) each value of $N_{10\text{-}500}$ lower than 1.1 times the median value of $N_{10\text{-}500}$ during 21 min; and (3) relative wind speed greater than 1 ms^{-1}. As an example, $N_{10\text{-}500}$ values before and after data screening of (1) and (2) are depicted as black dots in Fig. 2b. $N_{10\text{-}500}$ values before screening sometimes increased for a short time in a downwind condition, at the timing of relative wind (because of the ship's velocity or direction change and following exhaust) and at another condition (probably because of the effect of activity on ships or another ship). As a result of screening (1) and (2), the periods of rapid increase and high concentration of $N_{10\text{-}500}$ were omitted. Data near 1 m/s relative wind speed were also eliminated using a screening method (3) for safety because air masses under a calm environment had the possibility of contamination. This screening can accommodate effects by temporal exhaust such as kitchen exhaust and another ship's exhaust, and can also screen contamination from a backwards relative wind direction. In this study, a threshold by relative wind direction was not used to avoid the necessity of additional screening beyond the amount needed for this study. The 15 min average and daily average for the local time (based on the zenith time) were calculated after data screening.

2.2.2. Lognormal fitting

Number–size distributions of aerosol particles were approximated using a sum of up to three lognormal functions individually. The sum of the lognormal function is given as shown below.

$$\frac{dN}{d\log D_p} = \sum_{i=1}^{2or3} \frac{N_i}{\sqrt{2\pi}\log \sigma_{g,i}} \exp\left[-\frac{(\log D_p - \log D_{g,p,i})^2}{2\log^2 \sigma_{g,i}}\right]$$

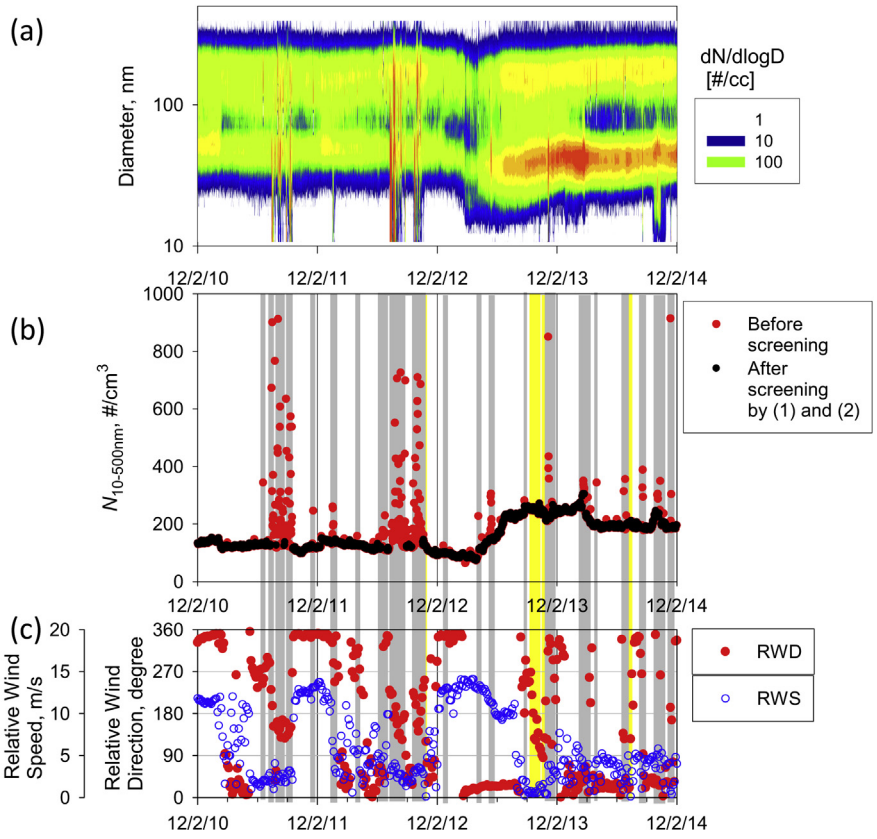

Fig. 2. Examples of (a) number–size distribution (dN/dlogD_p, cm^{-3}) of aerosol particles, (b) number concentration of 10–500 nm particles before and after data screening based on temporal variation of number concentration and (c) relative wind speed and direction. The light gray areas of (b) and (c) show the periods subject to screenings of (1) and (2). The yellow areas of (b) and (c) show the periods subject to screening of (3). (For interpretation of the references to colour in this figure legend, the reader is referred to the web version of this article.)

Therein, D_p signifies the particle diameter, $D_{g,p,i}$ denotes the modal geometric mean diameter, $\sigma_{g,i}$ is the modal geometric standard deviation, and N_i stands for the particle number concentration in mode i. Details of the lognormal distribution were described by Seinfeld and Pandis (2006). Generally, modes appearing in sub-micrometer sizes are called nucleation, Aitken, and accumulation modes according to their geometric mean diameter (Kulmala et al., 2004; Raes et al., 2000). For this study, we designated the modes in sub-micrometer sizes as follows: nucleation mode, $D_{p,g} < 30$ nm; Aitken mode, 30 nm $< D_{p,g} <$ 85 nm; and accumulation mode, $D_{p,g} > 85$ nm.

2.2.3. Condensation sink

The condensation sink (CS) is a measure of the scavenging speed of gaseous molecules caused by condensation onto particles, which depends on the particle size and condensation. CS is calculated using the following equation (Kulmala et al., 2001).

$$CS = 2\pi D_v \int_0^\infty D_p \beta_m(D_p) n(D_p) dD_p = 2\pi D_v \sum_i D_{p,i} \beta_{m,i} N_i$$

In that equation, D_v is the diffusion coefficient of the condensing vapor. The diffusion coefficient of H_2SO_4 vapor (0.077 cm^2/s^{-1}. Hanson and Eisele (2000) is used for calculations. In addition, $D_{p,i}$ and N_i respectively denote the central particle diameter and number concentration of size class i. The transitional correction factor $\beta_{m,i}$ can be expressed as (Fuchs and Sutugin, 1971)

$$\beta_{m,i} = \frac{Kn_i + 1}{0.377Kn_i + 1 + \frac{4}{3}\alpha^{-1}Kn_i^2 + \frac{4}{3}\alpha^{-1}Kn_i}$$

where the mass accommodation coefficient α is assumed as unity. The Knudsen number (Kn) is

$$Kn_i = \frac{2\lambda_v}{D_{p,i}},$$

where λ_v stands for the mean free path of condensing vapor molecule expressed as

$$\lambda_v = 3D_v\sqrt{\frac{\pi M_v}{8K_BT}}.$$

In that equation, M_v stands for the molecular mass of the condensing vapor, K_B represents Boltzmann's constant, and T denotes the air absolute temperature. In this study, although the aerosol number concentration was measured after drying, the condensation sink at ambient air would be higher by particle hygroscopic growth. Therefore, the CS for ambient relative humidity was also estimated using a growth factor (Seinfeld and Pandis, 2006), assuming that the respective compositions were H_2SO_4 for <0.5 μm particles and NaCl for >0.5 μm particles.

2.3. Observation of DMS in seawater and air

DMS concentrations in the surface seawater and atmosphere

were measured using a proton transfer reaction – mass spectrometry (PTR-MS; Ionicon Analytik GmbH, Innsbruck, Austria). The methods of measurements by PTR-MS on the ship were explained by Kameyama et al. (2009, 2010) and by Omori et al. (2013). Air from the upper deck on the ship was drawn through a borosilicate glass filter housing and 100 m of perfluoroalkoxy tubing (3/8″ O.D.) at approximately 30 L min^{-1} to the ship's laboratory. From that air flow, the air sample was introduced into PTR-MS at a flow rate of 100 sccm. The surface seawater pumped by the ship system from approximately 5 m depth flowed continuously into a 10-L glass equilibrator at 1 L min^{-1}. Ultrapure nitrogen flowed from the bottom to the upper outlet of the equilibrator at 120 sccm. It was introduced into PTR-MS. Dissolved DMS was extracted into the gas phase. Some of the DMS-containing extractant gas was directed continuously to the PTR-MS instrument at ambient pressure without pretreatment such as dehydration or pre-concentration. The mass signal of DMS in the sample gas was obtained at 5-s integration to obtain a mass signal at 1-min intervals. The detection sensitivity under dry conditions and the relation between the humidity and the detection sensitivity for DMS were ascertained using methods reported by Inomata et al. (2008) and by Kameyama et al. (2009). The DMS concentrations in the seawater sample were calculated from concentrations in the sample gas extracted from the equilibrator with Henry's law constant (Kameyama et al., 2009).

2.4. Air mass backward trajectories

Air mass backward trajectories were analyzed to investigate their relation to observed size distributions of aerosol particles. The backward trajectory and precipitation data were computed using the Hybrid Single-Particle Lagrangian Integrated Trajectory (HYSPLIT 4) model developed by the National Oceanic and Atmospheric Administration (NOAA) Air Resources Laboratory (ARL) (Draxler and Rolph, 2003; Rolph, 2003). Calculations of 120-h backward trajectories started from 500 m a.s.l. above the site every 3 h. The National Weather Service's National Centers for Environmental Prediction (NCEP) GDAS archive was used for meteorological input data. The cumulative precipitation amount was calculated from the hourly precipitation amount along the backward air mass trajectory by HYSPLIT model, based on the method described by Nishita et al. (2007). The HYSPLIT precipitation product has some limitations. Particularly, it does not account for boundary layer processes or convection. For this study, the precipitation data were used as an indicator for precipitation caused by large-scale uplift. However, it is noteworthy that it is not necessarily a good reflection of boundary layer drizzle that might be a significant form of precipitation.

3. Results and discussion

3.1. Temporal and horizontal variations of number–size distribution of aerosols and individual particle compositions

Fig. 3 portrays temporal variations of the number–size distribution ($dN/d\log D_p$, cm^{-3}) of aerosol particles and the modal geometric mean diameters ($D_{p,g,i}$) obtained using the lognormal fitting described above (Fig. 3a), the total number concentration of 10–500 nm particles by SMPS and the particle number concentrations in each mode by lognormal fitting (Fig. 3b), the number concentration of >0.1 μm particles by LPC (Fig. 3c), condensation sink of dried and ambient aerosols (CS) (Fig. 3d), ambient temperature and relative humidity (Fig. 3e), precipitation and cumulative precipitation amount experienced by air mass for the prior day and prior 3 days (Fig. 3f), and wind direction and speeds (Fig. 3g) during the observation period. Periods shown as white in Fig. 3a are periods that were unavailable by data screening because of failure of instrumentation and EEZ regions of the USA, Ecuador, and Peru. The ocean areas are shown at the top of Fig. 3a. The number concentrations of 10–500 nm and >0.5 μm particles, wind speed, and number concentration and modal diameters of each mode are also shown as horizontal variation in Fig. 4.

The number–size distribution and total number concentration of 10–500 nm particles changed during a few-dozen days in remote ocean areas, but included no sudden change (Fig. 3a and b). That result shows that the backward data were extractable by the screening. The total number concentration of aerosol particles with diameter of 10–500 nm on the open sea was stable, 100–400 cm^{-3}, which was about one order of magnitude lower than the figures obtained around Tokyo and Honolulu (Fig. 3b). Throughout the observed remote ocean areas, the number–size distributions of the submicrometer particles were found to be bi-modal distributions with valleys at 50–100 nm and peaks at 30–60 nm and 100–200 nm: Aitken and accumulation modes were dominant in terms of both frequency of occurrence and modal concentration. Although the variation of the accumulation mode was smaller (Fig. 4f), the mode diameters of Aitken mode and the number concentrations varied greatly according to the area and period (Fig. 4e). Especially, greater mode diameters of Aitken particles were observed constantly around the equator area (Fig. 4e). Heintzenberg et al. (2000) reviewed the size distributions of marine aerosols and reported that the modal diameter of Aitken mode in low latitude ocean areas (approx. 47 nm at 15°N–15°S) tended to be higher than that at higher latitudes. The occurrence of nucleation mode particles was rare at the equator area during this study, although it occurred more frequently at mid-latitudes in both the North Pacific and South Pacific (Fig. 4d). For coarse particles of >0.5 μm diameter, number concentrations were 1–10 cm^{-3} (Figs. 3c and 4b). They were poorly correlated with those of 10–500 nm particles. The number concentrations of >0.5 μm particles were often high in the North Pacific, but those at the equator and the South Pacific were low and stable values. Wind speeds (Fig. 4c) were also low (<5 ms^{-1}) at the equator and in the South Pacific. The mass concentrations of sea-salt aerosol particles derived from the ocean are known to show correlation with wind speed (Lewis and Schwartz, 2004). In this study, the number concentrations of coarse (>0.5 μm) particles tended to be higher at higher wind speeds (Figs. 3g and 4b). Fig. 5 presents the relation between wind speed and number concentration of each size range for remote ocean areas (2–20 December 2011, 27 December 2011–24 January 2012, 31 January 2012–17 February 2012 and 24 February 2012–4 March 2012). Correlation with >0.5 μm particles (Fig. 5d) was high ($R^2 = 0.45$ and $R_s = 0.688$). Although some simulation models incorporate accumulation mode sea salt emissions (Clarke et al., 2006; Gong, 2003), clear positive correlation between the number concentrations of fine (<0.5 μm) particles and wind speed was not found in this study (Fig. 5a–c). The number concentration of 30–85 nm particles were sometimes higher in weak wind speed, consequently showing a weak negative correlation (Fig. 5b). Fig. 3 shows that the higher number concentrations of 30–85 nm particles (200–400 #/cm^3) were observed for certain long periods (12–18 Jan 2012, and 13–16 Feb), as depicted in Fig. 3. Because the number-size distributions of the periods maintained a similar concentration and shape, the concentration of Aitken mode particles was high. This observation included various regions with topographic and meteorological properties. Meteorological, oceanic, and atmospheric properties can differ among regions. Consequently, the number concentrations of respective size ranges might also differ according to wind speed.

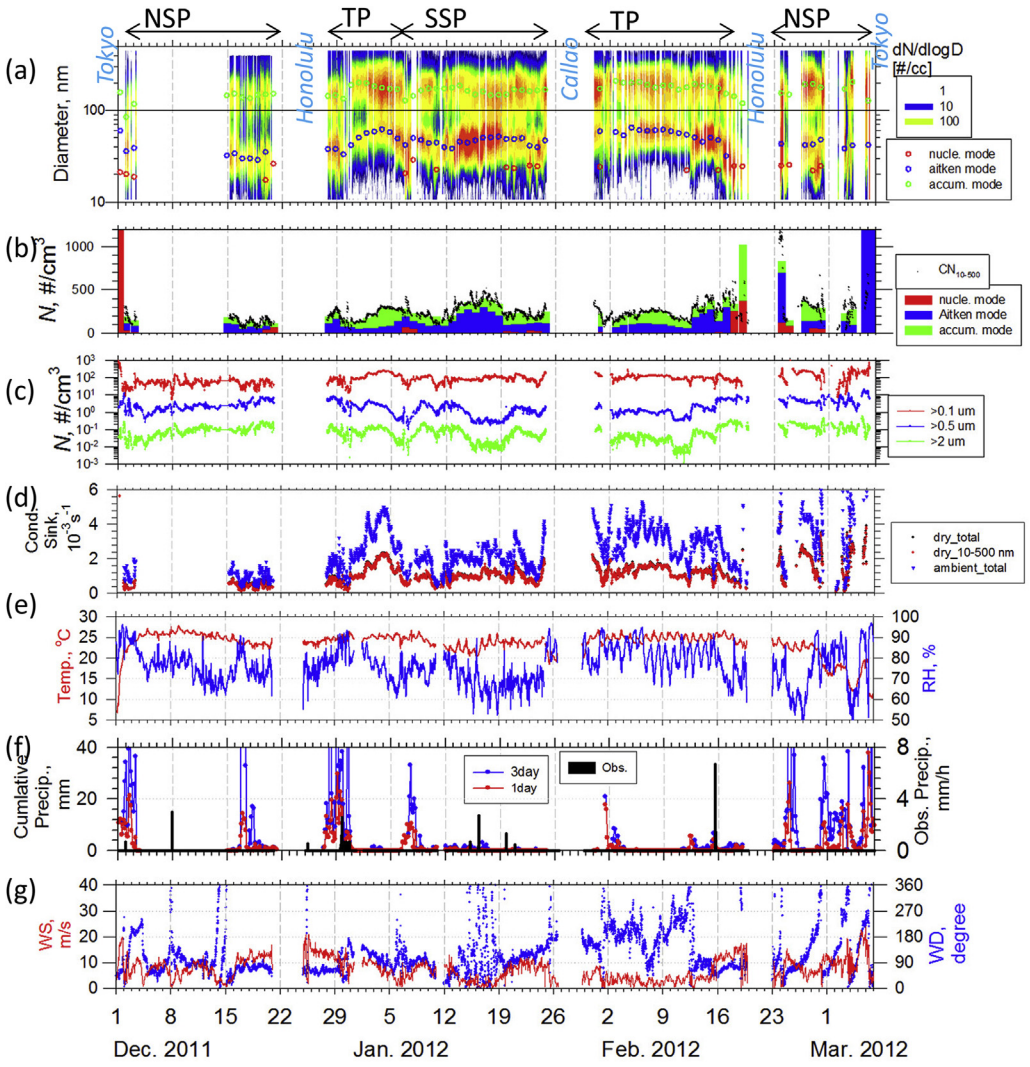

Fig. 3. Temporal variations of (a) number–size distribution ($dN/d\log D_p$, cm^{-3}) of aerosol particles and the modal geometric mean diameters ($D_{p,g,i}$) obtained by lognormal fitting, (b) total number concentration of 10–500 nm particles by SMPS and particle number concentrations in each mode by lognormal fitting, (c) number concentration of >0.1 μm particles by LPC, (d) condensation sink (*CS*) of dried 10–500 nm particles (red dot), dried total particles (black dot) and ambient total particles (blue dot), (e) ambient temperature and relative humidity, (f) observed precipitation intensity and cumulative precipitation amount experienced by air mass for the preceding 1 day and 3 days, and (g) wind direction and speeds. The horizontal black bar in (a) shows the region of the north subtropical Pacific area (NSP), the tropical Pacific area (TP), and the south subtropical Pacific area (SSP). (For interpretation of the references to colour in this figure legend, the reader is referred to the web version of this article.)

3.2. Classification of number–size distributions by area and features

As explained in the preceding section, most number–size distributions were observed as bi-modal distributions, but the features of the distribution, particularly in the Aitken mode, differed according to the area and period. To discuss factors affecting the number–size distribution of remote maritime aerosols, we organized a number–size distribution by the ocean area and features. Referring to the horizontal variation of number–size distribution, the observed areas were classified into 20°N–40°N as the north subtropical Pacific area (NSP), 15°N–15°S as the tropical Pacific area (TP), and 15°S–40°S as the south subtropical Pacific area (SSP). Fig. 6 portrays the number–size distribution classified by the shape and observation area. Number–size distributions of two types were found for each area. Tables 1–3 present details of the averaged fitting parameters of the number–size distribution for each ocean area.

In the NSP, the number concentrations of 10–500 nm particles, particularly accumulation mode particles, were low during December 2011. During 2012, although the number concentrations were low on 24 February and 3 March 2012, the number concentrations were often higher than 250 cm^{-3}. They were dominant in accumulation mode. The number–size distributions for which number concentrations of 10–500 nm were <250 cm^{-3} in NSP are shown in Fig. 6a as NSP1. The other type is shown in Fig. 6b as NSP2. The mode diameters of accumulation and Aitken modes of NSP1, with respective average diameters of 139 nm and 33 nm, were smaller than those of other areas. In the TP, properties of the number–size distribution differed west and east of 135°W. For the number–size distribution west of 135°W, as shown in Fig. 6 as TP1, mode sizes of Aitken mode particles on all days were less than 50 nm. The number concentration of Aitken mode varied from 66 #/cm^3 to 122 #/cm^3. For areas east of 135°W, shown in Fig. 6 as TP2, mode sizes of Aitken mode particles on all days were greater than 50 nm. Temporal and horizontal variation of the number size distribution were less. The respective mode sizes of Aitken and accumulation modes were 50–64 nm and 167–207 nm, which were larger than those of other areas, suggesting that particles were

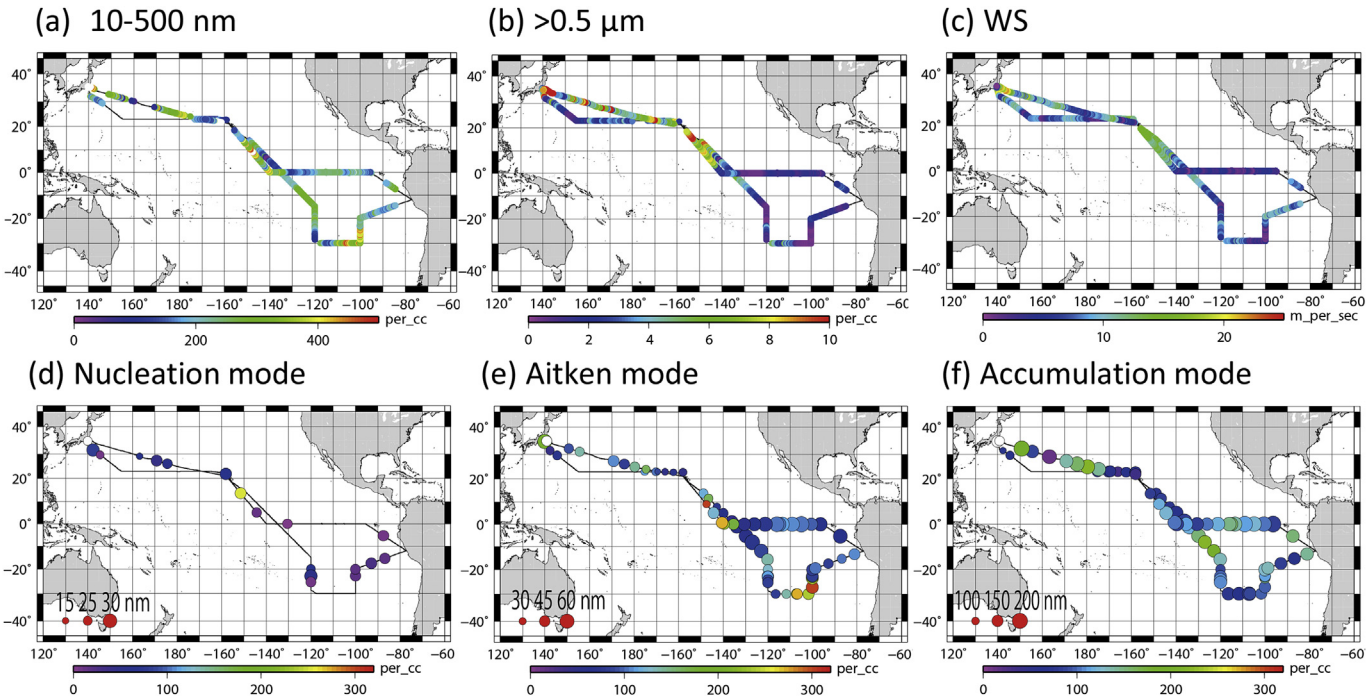

Fig. 4. Horizontal variation of (a) number concentrations of 10–500 nm, (b) number concentration of >0.5 μm particles, (c) wind speed, and number concentration, and (d, e, and f) number concentration (color) and modal diameters (dot size) of nucleation mode, Aitken mode, and accumulation mode particles.

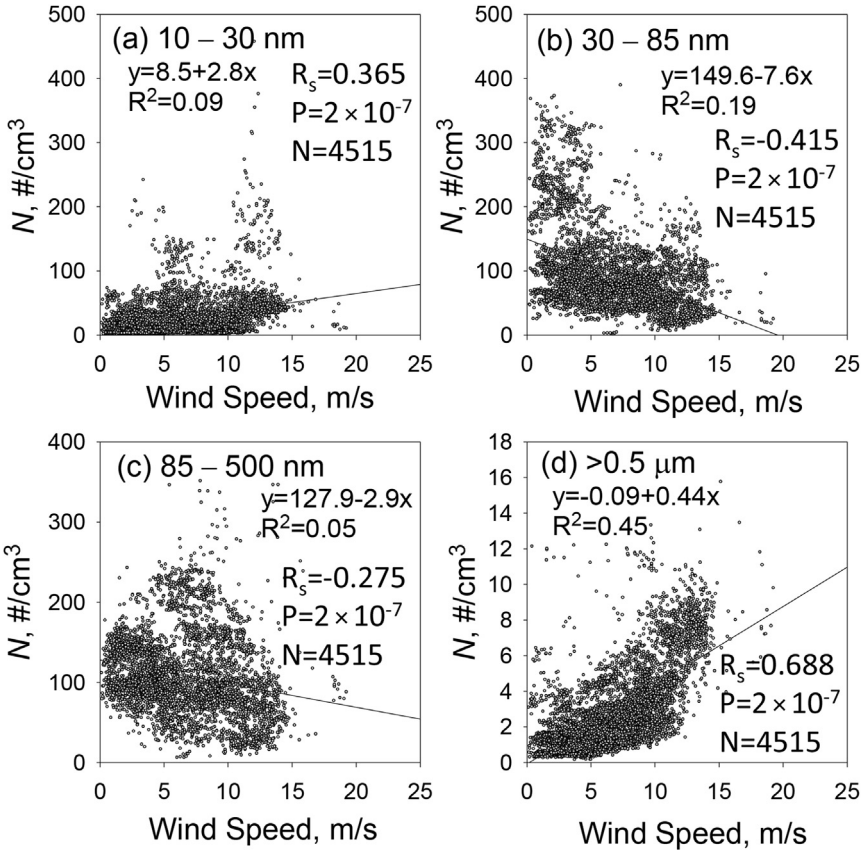

Fig. 5. Relations between wind speed and number concentrations of (a) 10–30 nm particles, (b) 30–85 nm particles, (c) 85–500 nm particles, and (d) > 5 μm particles. Expressions and R^2 respectively represent linear regression results and the squared collation coefficient. *Rs*, *P* and N^2 respectively represent the correlation coefficient of Spearman-rank-order-correlation test, the *P* value, and the number of samples.

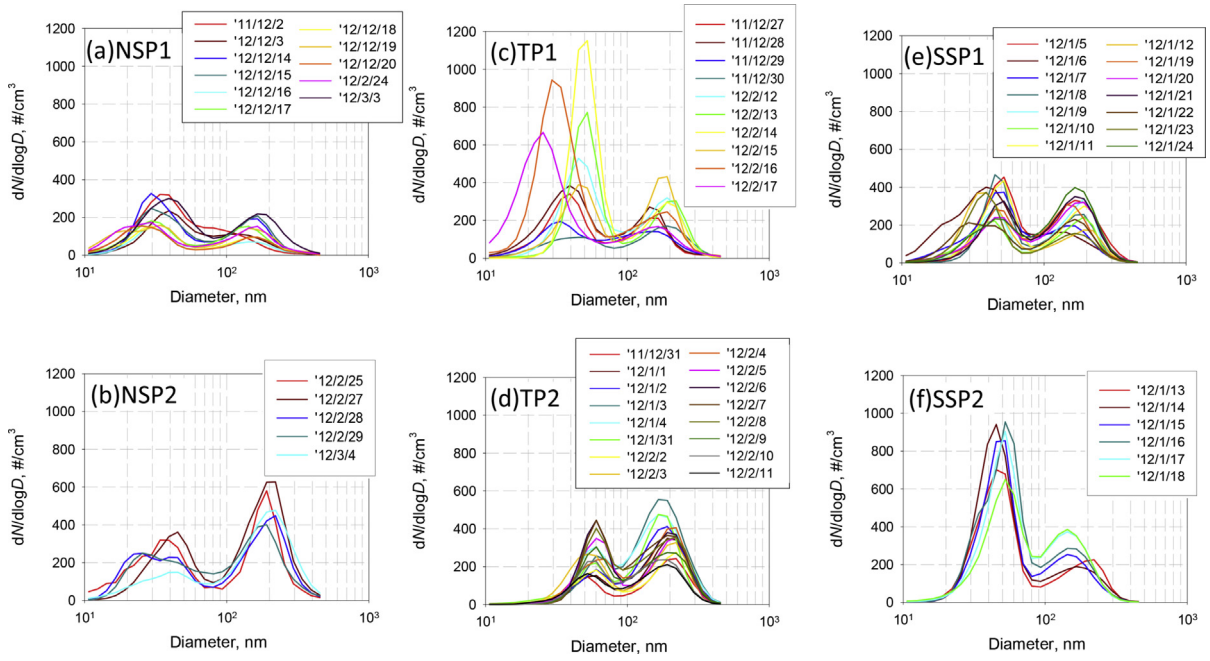

Fig. 6. Number–size distributions classified by the shape and observation area. Observed areas were classified: 20°N–40°N as the north subtropical Pacific area (NSP), 15°N–15°S as tropical Pacific area (TP), and 15°S–40°S as the south subtropical Pacific area (SSP).

Table 1
Average modal parameters (modal geometric mean diameter $D_{g,p,i}$, modal geometric standard deviation $\sigma_{g,i}$, and particle number concentration N_i in mode i) for different air masses classified by shapes of number–size distributions of the north subtropical Pacific area (NSP).

		N_i [cm^{-3}]	$D_{g,p,i}$ [nm]	$\sigma_{g,i}$	Observed number of days (%)
NSP all	Accumulation mode	94.6 ± 54.5	154.7 ± 29.8	1.18 ± 0.04	16 (100%)
	Aitken mode	94.3 ± 33.7	36.0 ± 5.3	1.19 ± 0.05	14 (88%)
	nucleation mode	47.8 ± 23.7	21.8 ± 3.2	1.16 ± 0.03	7 (44%)
NSP1	Accumulation mode	60.8 ± 16.3	138.9 ± 21.4	1.20 ± 0.03	11 (100%)
	Aitken mode	81.9 ± 29.3	33.2 ± 3.4	1.16 ± 0.03	9 (82%)
	Nucleation mode	47.0 ± 27.8	21.2 ± 3.5	1.17 ± 0.03	5 (45%)
NSP2	Accumulation mode	168.8 ± 30.3	189.6 ± 8.6	1.15 ± 0.02	5 (100%)
	Aitken mode	116.5 ± 29.6	41.1 ± 4.2	1.23 ± 0.05	5 (100%)
	Nucleation mode	49.7 ± 5.9	23.1 ± 1.4	1.13 ± 0.01	2 (40%)

* ± values are standard deviations.

Table 2
Average modal parameters for different air masses classified by shapes of number–size distributions of the tropical Pacific area (TP).

		N_i [cm^{-3}]	$D_{g,p,i}$ [nm]	$\sigma_{g,i}$	Observed number of days (%)
TP all	Accumulation mode	115.9 ± 37.7	176.6 ± 19.8	1.16 ± 0.03	26 (100%)
	Aitken mode	111.7 ± 65.9	51.6 ± 9.3	1.15 ± 0.03	25 (96%)
	Nucleation mode	68.9 ± 106.8	23.0 ± 1.1	1.12 ± 0.04	4 (15%)
TP1	Accumulation mode	92.6 ± 19.0	161.3 ± 19.8	1.18 ± 0.04	10 (100%)
	Aitken mode	168.1 ± 79.5	40.8 ± 6.1	1.16 ± 0.04	9 (90%)
	Nucleation mode	132.8 ± 121.0	23.2 ± 1.2	1.14 ± 0.03	2 (20%)
TP2	Accumulation mode	130.5 ± 39.1	186.2 ± 12.4	1.16 ± 0.02	16 (100%)
	Aitken mode	79.9 ± 21.0	57.7 ± 3.5	1.14 ± 0.03	16 (100%)
	Nucleation mode	5.0 ± 3.2	22.8 ± 1.0	1.10 ± 0.03	2 (13%)

aged well. In the south subtropical Pacific area (SSP), number concentrations of 10–500 nm were mostly around 250 cm^{-3}, except during 13–18 January 2012. The number–size distributions of 13–18 January 2012 and the others in the SSP were classified respectively as SSP 2 and SSP1, as shown in Fig. 6e and f. Number concentrations of SSP1 were comparable in Aitken and accumulation modes. The nucleation mode was found occasionally in the SSP1. In SSP2, the number concentrations of Aitken mode particles were higher and moderate.

3.3. Relations of number–size distribution with air mass trajectories, meteorological conditions, and marine chlorophyll concentrations

The air mass trajectories of each classified number–size distribution had common trends for route and meteorological conditions. Figs. 7 and 8 respectively portray the horizontal backward air mass trajectory and vertical backward air mass trajectory with hourly precipitation amounts along the route that was classified

Table 3
Average modal parameters for different air masses classified by shapes of number–size distributions of the south subtropical Pacific area (SSP).

		N_i [cm^{-3}]	$D_{g,p,i}$ [nm]	$\sigma_{g,i}$	Observed number of days (%)
SSP all	Accumulation mode	103.0 ± 24.3	160.2 ± 13.5	1.16 ± 0.02	20 (100%)
	Aitken mode	144.8 ± 71.3	45.4 ± 4.0	1.14 ± 0.03	20 (100%)
	Nucleation mode	29.1 ± 20.6	23.7 ± 2.3	1.16 ± 0.03	7 (35%)
SSP1	accumulation mode	101.0 ± 24.6	161.5 ± 13.2	1.17 ± 0.02	14 (100%)
	Aitken mode	100.9 ± 19.8	44.4 ± 4.0	1.15 ± 0.03	14 (100%)
	nucleation mode	29.1 ± 20.6	23.7 ± 2.3	1.16 ± 0.03	7 (50%)
SSP2	accumulation mode	107.6 ± 23.2	157.1 ± 13.8	1.16 ± 0.02	6 (100%)
	Aitken mode	247.2 ± 32.1	47.6 ± 2.8	1.13 ± 0.01	6 (100%)
	Nucleation mode	–	–	–	0 (0%)

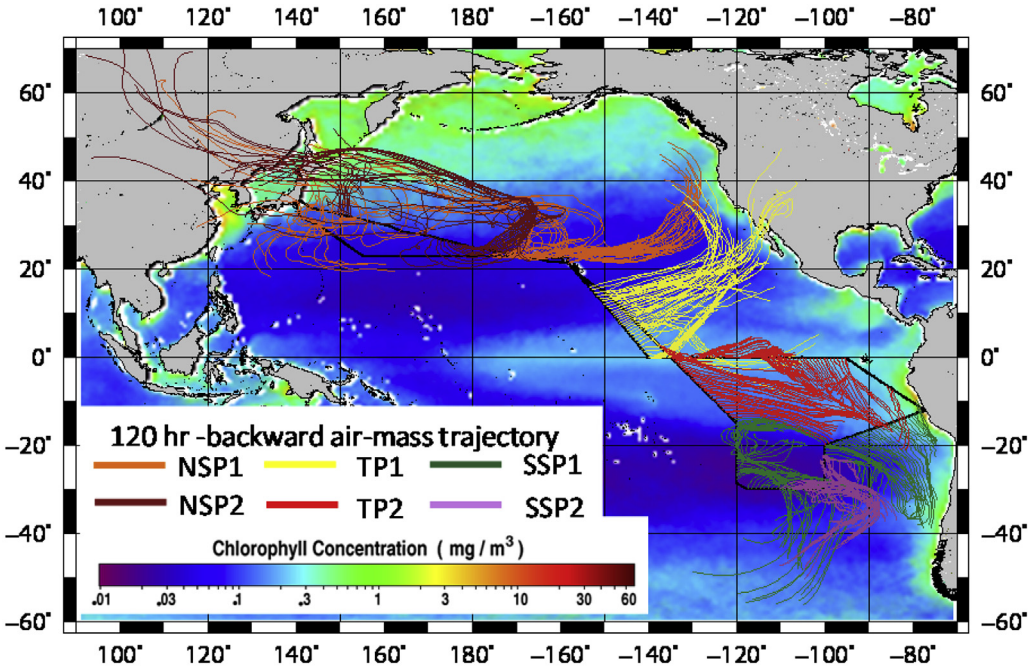

Fig. 7. Horizontal backward air mass trajectory classified corresponding to the same categories of number–size distribution as those of Fig. 6. Ocean area color depicts the averaged chlorophyll α concentrations (surface water biological activity) in the observation period of MODIS satellite (NASA/Goddard Space Flight Center).

corresponding to the same categories of the number–size distribution presented in Fig. 6. Area colors of Fig. 7 depict averaged chlorophyll α concentrations (surface water biological activity) during the observation period of moderate resolution imaging spectroradiometer (MODIS) satellite images provided by the NASA/Goddard Space Flight Center. Based on horizontal and vertical trajectory analysis (Figs. 7 and 8), the air masses for the classified number–size distribution of each area exhibited the following tendencies: the air mass of NSP1 was derived from the direction east or south of the sea region of low chlorophyll concentrations in the boundary layer (mostly under 2000 m a.s.l.), that of NSP2 from eastern Asia at high altitude (>3000 m a.s.l. before 3 days) moving clockwise to the observation site, that of TP1 from direction of the northeast, that of TP2 from east or southeast of the sea region of higher chlorophyll α concentrations in the boundary layer under 2000 m a.s.l., and that of SSP (SSP1 and SSP2) from the southeast in the boundary layer under 2000 m a.s.l., moving clockwise to the site. Some previous studies described that local subsidence and entrainment efficiently affect the atmosphere in the MBL (Clarke et al., 1996; 1998b). Clarke et al. (1996) estimated the entrainment rate into the MBL over equator based on ozone fluctuations. Table 4 shows the average concentration of CO and O_3 according to the ocean area and shapes of the number–size distribution. CO is emitted by combustion. The O_3 source is mainly stratospheric chemistry and artificial source. The CO concentration of NSP was high, whereas that of SSP and TP2 was low, suggesting that air masses of SSP and TP2 were less affected by emissions from industrial activity. For the ratio of O_3 to CO, that of NSP and TP1 was higher than that of TP2 and SSP. The results of vertical trajectories and trace gas concentrations suggest that the air mass of NSP and TP1 is more strongly affected by subsidence and entrainment from above the MBL. Precipitation along the trajectories (Fig. 8) exhibited high frequency and high intensity for air masses derived from the northern hemisphere (NSP1, NSP2, and TP1). However, those around the equator or from the southern hemisphere were less so, although some low-intensity precipitation was experienced for the SSP1 air mass. The number–size distribution can be formed mainly by particle formation, growth, and scavenging. Relations with clouds are explained in section 3.4. Additionally, particle formation related to the number concentration of nucleation and small Aitken particles is described in Section 3.4.

Sensitivity of the particle number concentration to precipitation amounts along the trajectory route was also reported for the number–size distribution observed at Mt. Norikura, Japan (Nishita

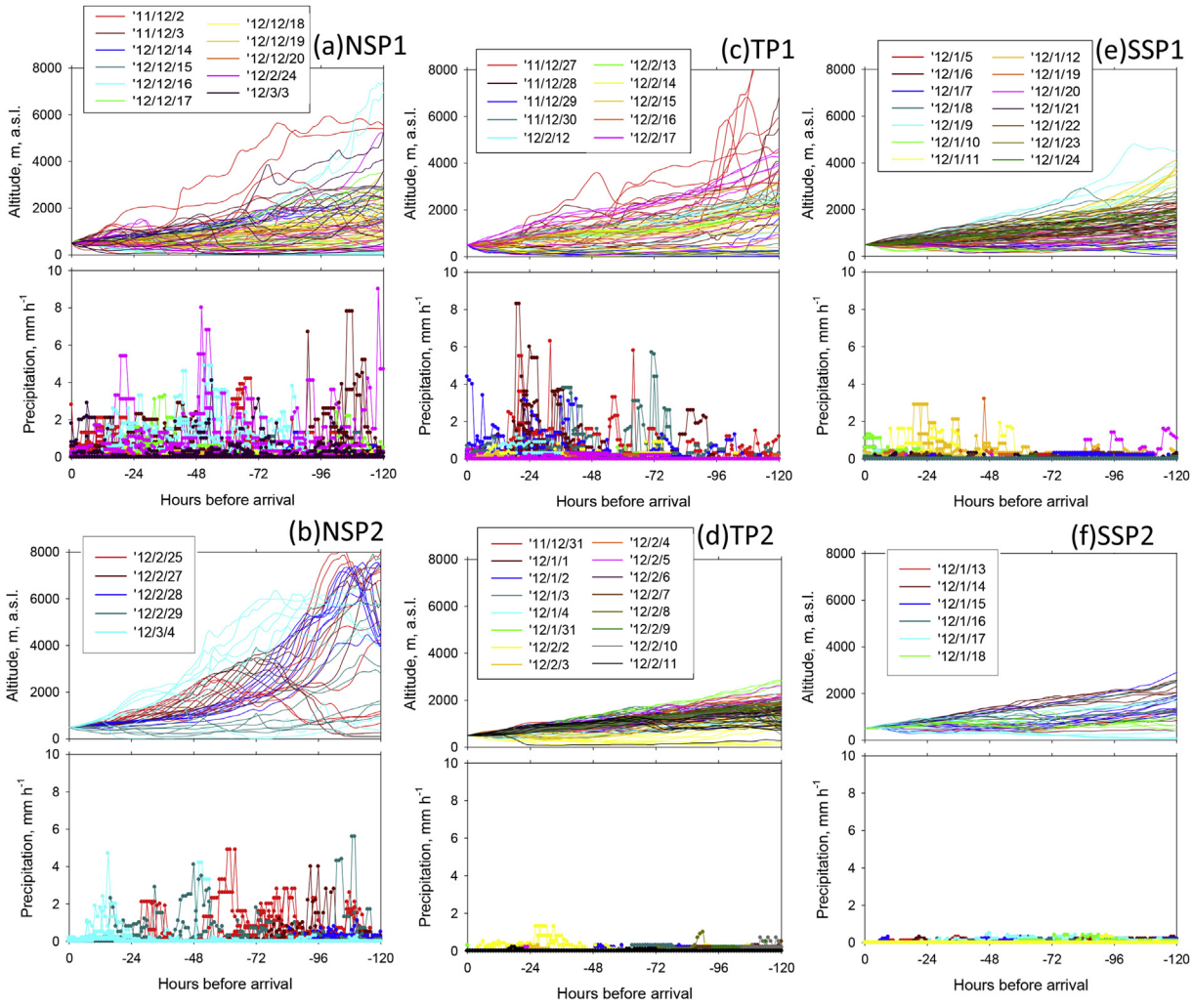

Fig. 8. Vertical backward air mass trajectory with hourly precipitation amounts along the route. Panels are classified corresponding to the same categories of the number–size distribution as those shown in Fig. 6.

Table 4
Average concentrations of trace gass for different air masses classified by ocean area and shapes of number–size distributions.

		CO [ppbv]	O_3 [ppbv]	O_3/CO
NSP	NSP1	116.5 ± 31.1	24.2 ± 8.4	0.22 ± 0.08
	NSP2	165.7 ± 22.8	35.8 ± 6.3	0.22 ± 0.03
	All	130.6 ± 36.5	27.7 ± 9.5	0.22 ± 0.07
TP	TP1	99.2 ± 21.2	17.3 ± 6.6	0.18 ± 0.08
	TP2	64.0 ± 9.8	6.2 ± 4.5	0.10 ± 0.07
	All	78.5 ± 23.3	10.7 ± 7.7	0.13 ± 0.08
SSP	SSP1	55.2 ± 10.9	6.3 ± 2.9	0.12 ± 0.08
	SSP2	53.5 ± 7.4	6.5 ± 1.4	0.12 ± 0.03
	All	54.7 ± 10.0	6.4 ± 2.5	0.12 ± 0.06

et al., 2007). Nishita et al. (2007) reported a negative correlation of the logarithm of the number concentration of 100–300 nm particles with cumulative day precipitation amounts, although the correlation of 9–100 nm was less. They suggested that the sensitive decrease of the concentration of 10–300 nm resulted from in-cloud scavenging processes by comparison of their estimated e-folding time and the value of simulation studies by Scott (1982) and Andronache (2004). In this study, in the northern hemisphere, where the precipitation intensity and frequency along the trajectories were high with high O_3 ratio, the number concentrations of accumulation mode of NSP1 were especially lower. Furthermore, the mode diameter of accumulation mode of NSP1 was smaller. Such a size distribution might be attributed to in-cloud scavenging and localized subsidence and entrainment enhanced around the convective clouds. The trajectory route of NSP1 also passed through the north oligotrophic sea area. Therefore, in addition to scavenging by precipitation, particle growth is not expected. Nevertheless, the NSP2 in the continental air mass from

eastern Asia via high altitude exhibited a larger number concentration of accumulation mode particles. The anthropogenically influenced air over the continent might affect the number concentration. Although the relation with precipitation is less clear, the number concentration of the accumulation mode of TP1 also tended to be less for air masses that experienced high-intensity precipitation at lower altitudes (27–30 December 2011). Higher number concentrations of Aitken mode in TP1 (12–15, and 17 February 2012) also corresponded with air masses from higher altitudes, which experienced less precipitation. This fact is discussed in relation to new particle formation in Section 3.4.

Air masses from the equator and southern hemisphere were less affected by precipitation. Their vertical trajectory remained at low altitude. Particularly for TP2 and SSP2, the observed precipitation and the precipitation along the trajectory were very slight. However, the number–size distribution exhibited differences of size and concentration of Aitken mode in each sea area. The observed bimodal distribution in TP2 had a lower number concentration but a larger size of Aitken mode, which can be regarded as more aged. Raemdonck et al. (1986) also observed aerosol chemical composition over the equator of the south east ocean by ship observation. They reported that selenium levels in the remote equator had high concentration, suggesting an effect of the biological source. In addition, the concentrations of excess sulfate were found to be consistent with the flux of dimethylsulfide. Although some key factors exist related to growth processes of Aitken mode, the air mass of TP2 in this study remained over the ocean area of especially high chlorophyll concentration. If the particles were affected by the condensation of gaseous materials emitted by marine biological gaseous, then without removal by precipitation scavenging, it is reasonable to expect that particles would be larger over the equator.

3.4. New particle formation events: properties and occurrence frequencies in different ocean areas

Observation conducted for this study showed that nucleation mode particles often appeared over the mid-latitude western North Pacific area and the mid-latitude eastern South Pacific area. Occurrences of the nucleation mode attributed to new particle formation (NPF) events were observed frequently. The NPF includes homogeneous nucleation and subsequent particle growth, which are important source processes to increase the number concentrations of aerosol particles and cloud condensation nuclei in the atmosphere (Kerminen et al., 2005; Lihavainen et al., 2003). However, observation studies have difficulty measuring particles having immediate diameter of nucleation: a few nanometers. In previous observation study, the growth events of nucleation mode particles have been treated as NPF events, which suggests that nucleation occurred at a proximal time and area (Nishita et al., 2008). In this study, an NPF event is defined as that which first appears at sizes smaller than 20 nm diameter and for which growth is observed continuously for longer than 1 h according to the method reported by Dal Maso et al. (2005).

As an example of observed NPF events over the South Pacific in this study, temporal variations of the solar irradiation, the number–size distribution at 3 min time resolution and the fitting results at 19 and 20 February 2012 are shown in Fig. 9. For NPF events of 19 February, a nucleation mode having a peak of less than 20 nm appeared during the daytime, although the number concentration was less than in Aitken and accumulation modes. The nucleation mode subsequently grew to larger than 30 nm and joined with Aitken mode over half a day. Furthermore, on 20 February, nucleation mode particles having a peak of less than 20 nm appeared in the morning and grew during about half a day. In this study, 13

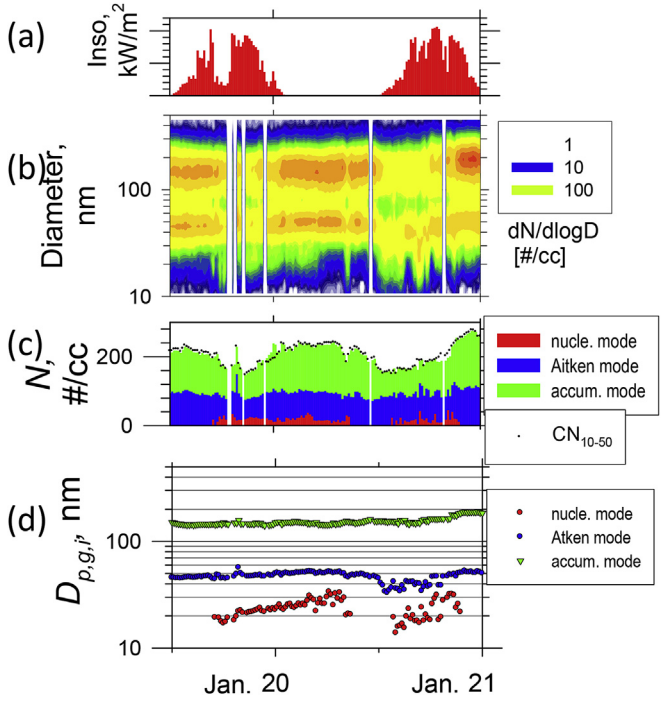

Fig. 9. Solar irradiation and number–size distributions for NPF events at 19 and 21 January: (a) solar irradiation, (b) number–size distribution ($dN/d\log D_p$, cm^{-3}) of aerosol particles, (c) particle number concentrations in each mode and total number concentrations of 10–500 nm particles, and (d) modal geometric mean diameters ($D_{p,g,i}$) obtained from lognormal fitting.

cases were observed as NPF events. Fig. 10 shows the number–size distributions, CS, and meteorological conditions for NPF event. Details of NPF events are presented in Table 5 for NSP and TP and in Table 6 for SSP. Table 7 presents DMS, CS, and the number (fraction) of NPF events for each area. In this observation, NPF events were frequently found over SSP (40% of observation days) whereas the fraction in TP was less. In most cases, nucleation mode particles appeared suddenly and grew to Aitken mode during a short time: within a day. Minimum diameters around the event start for each event were 12–19 nm (Tables 5 and 6). New particle formation should start at a few nanometers. Start diameters of some events were almost at the diameter limit of approximately 10 nm in our measurement. For larger minimum diameter (ca. 15 nm), the NPF events could be measured in the middle of the events because of movements of ships and air masses. The local-time temporal variation of solar irradiation and modal diameters of nucleation modes and linearization are depicted in Fig. 11. Previous reports have described that new particle formation events tend to occur along with solar radiation (Nishita et al., 2008). This occurrence is attributed to nucleation triggered by photochemical reaction. In addition, by condensation and coagulation processes, the particle size in an NPF event generally changes exponentially with a banana shape (Iida et al., 2008): initial nucleation particles grow faster, but the growth rate falls concomitantly with growth. A perfect 'banana' growth event occurs when the whole region upwind of the measurement site undergoes synchronized and homogeneous nucleation and growth event. So little is known about the fundamental processes that it cannot necessarily be assumed. Therefore, the growth becomes almost linear for particles larger than around 10 nm. This study found 10 cases of NPF events (6, 7, 19, 20, 22, and 23 January 2012 and 15, 17, 24, and 28 February 2012) during solar irradiation. Curves of less than 10 nm estimated from observed growth of greater than 10 nm could have converged to around

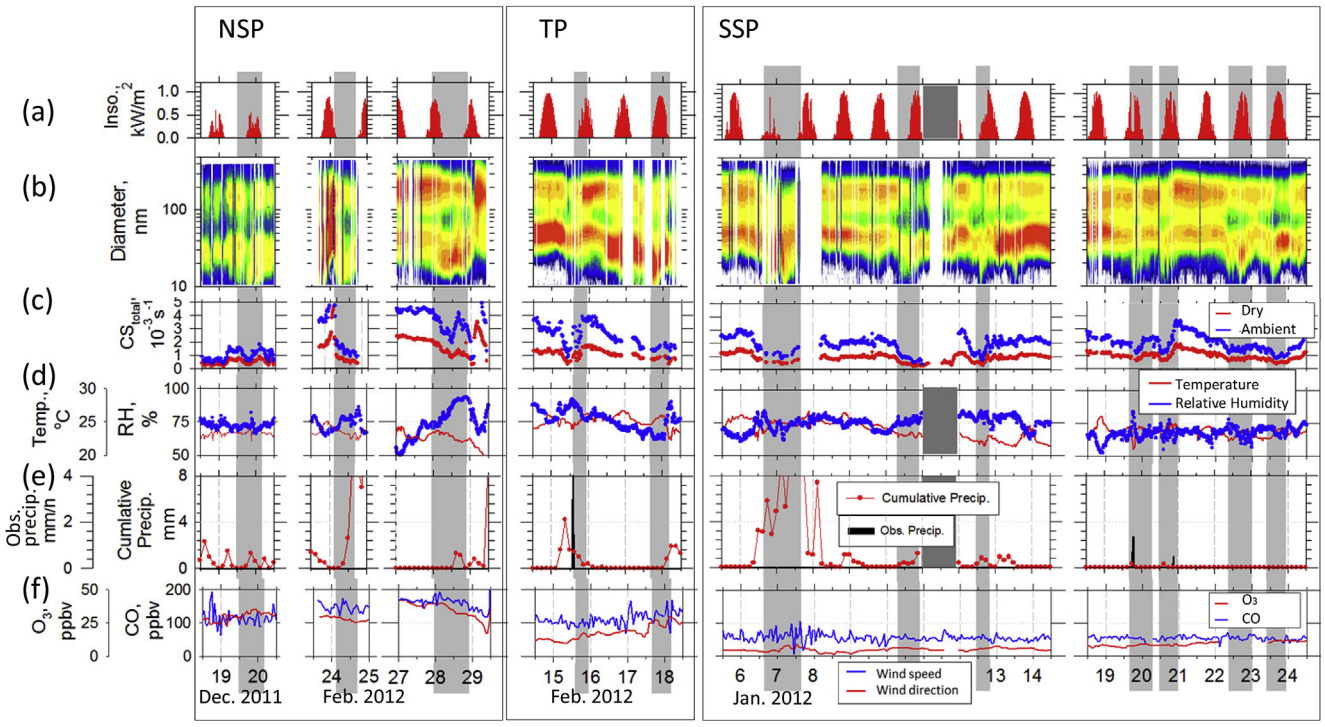

Fig. 10. Number–size distributions, condensation sink (*CS*) and meteorological conditions for NPF events: (a) solar irradiation, (b) number–size distribution ($dN/d\log D_p$, cm^{-3}) of aerosol particles, (c) *CS* of dried total particles and ambient total particles, (d) ambient temperature and relative humidity, (e) observed precipitation intensity and cumulative precipitation amount experienced by air mass for the prior 1 day and (f) ozone and carbon monoxide concentration. The light gray area shows the NPF event period. Number–size distribution of (b) is shown using the same color range as that used for Fig. 9b.

Table 5
Summary of new particle formation (NPF) events in a remote area over the north subtropical Pacific area (NSP) and the tropical Pacific area during KH-11-10 and KH-12-1 observations.

Start [UT] (local time[a])	End [UT]	Lat.	Long.	$D_{g,p,i}$ of nucle. mode[b]	*GR*	$N_{nucle.}$ avg. (max)	*CS* (CS_{amb}[c])	DMS concentration	
								Sea water	Atmos.
		[°N]	[°E]	[nm]	[nm/hr]	[cm^{-3}]	[$10^{-3}s^{-1}$]	[nM]	[ppb]
NSP									
2011/12/19 15:45 (5:12)	2011/12/20 11:45	22.8	−158.1	12–26	0.5	42 (86)	0.50 (1.06)	1.19	0.17
2012/2/24 4:30 (17:26)	2012/2/24 13:00	22.5	−165.8	16–28	0.6	58 (126)	0.64 (1.39)	1.75	0.17
2012/2/28 1:45 (13:19)	2012/2/28 20:00	26.6	173.6	19–25	0.2	90 (162)	1.24 (3.07)	5.90	0.19
TP									
2012/2/15 15:45 (6:08)	2012/2/15 23:45	5.0	−144.2	15–30	1.8	17 (32)	1.37 (3.18)	2.85	0.40
2012/2/17 17:00 (6:53)	2012/2/18 5:30	13.8	−151.7	19–30	1.0	241 (461)	0.74 (1.48)	3.49	–

[a] Local time is Universal time [hr] plus 24 [hr] × longtitude [deg]/360 [deg].
[b] Values indicate start–end diameter.
[c] CS_{amb} denotes *CS* for ambient relative humidity assuming composition of H_2SO_4 for <0.5 μm particles and NaCl for >0.5 μm particles.

Table 6
Summary of new particle formation (NPF) events in a remote area over the south subtropical Pacific area (SSP) during KH-11-10 and KH-12-1 observations.

Start [UT] (local time)	End [UT]	Lat.	Long.	$D_{g,p,i}$ of nucle. mode [nm]	*GR* [nm/hr]	$N_{nucle.}$ avg. (max)	*CS* (CS_{amb})	DMS concentration	
								Sea water	Atmos.
		[°N]	[°E]			[cm^{-3}]	[$10^{-3}s^{-1}$]	[nM]	[ppb]
SSP									
2012/1/6 17:30 (9:29)	2012/1/7 1:45	−20.0	−120.0	14–21	0.7	87 (250)	0.54 (1.19)	–	0.27
2012/1/7 2:00 (18:00)	2012/1/7 15:00	−21.9	−120.0	18–28	0.6	73 (224)	0.52 (1.15)	3.83	0.27
2012/1/10 10:30 (2:30)	2012/1/10 21:30	−26.9	−120.0	13–27	1.1	19 (74)	0.36 (0.79)	1.12	0.21
2012/1/12 12:00 (4:28)	2012/1/12 18:45	−30.0	−112.8	12–27	2.7	28 (75)	0.54 (1.26)	1.13	0.18
2012/1/19 17:30 (10:49)	2012/1/20 8:00	−22.4	−100.0	18–32	0.8	19 (37)	0.91 (1.89)	–	0.23
2012/1/20 13:45 (7:05)	2012/1/20 20:45	−20.0	−100.0	14–31	0.8	17 (45)	0.78 (1.59)	6.90	0.45
2012/1/22 14:00 (7:48)	2012/1/22 21:30	−17.6	−92.9	13–30	0.9	85 (190)	0.69 (1.41)	3.48	0.31
2012/1/23 14:15 (8:26)	2012/1/23 19:30	−15.5	−87.0	15–30	2.4	48 (84)	0.42 (0.87)	5.23	0.29

Table 7
DMS concentration, condensation sink, and observed number of NPF events for respective areas.

		DMS		CS,		NPF event day
		Surface seawater [nM]	Atmosphere [ppb]	Dry [10^{-3} s^{-1}]	Ambient [10^{-3} s^{-1}]	Count (%)
NSP	NSP1	1.26 ± 0.26	0.17 ± 0.06	0.50 ± 0.33	1.08 ± 0.80	2
	NSP2	1.76 ± 3.31	0.18 ± 0.03	1.91 ± 0.77	3.86 ± 1.27	1
	All	1.43 ± 1.95	0.18 ± 0.05	1.03 ± 0.87	2.00 ± 1.63	3(19%)
TP	TP1	3.17 ± 1.00	0.32 ± 0.11	0.98 ± 0.33	2.24 ± 0.82	2
	TP2	3.18 ± 0.82	0.25 ± 0.10	1.40 ± 0.41	3.25 ± 0.90	0
	All	3.17 ± 0.91	0.27 ± 0.11	1.24 ± 0.43	2.89 ± 0.99	2(8%)
SSP	SSP1	3.72 ± 1.85	0.30 ± 0.11	0.90 ± 0.34	1.81 ± 0.73	8
	SSP2	1.87 ± 0.45	0.19 ± 0.07	1.03 ± 0.17	2.18 ± 0.34	0
	All	3.08 ± 1.76	0.27 ± 0.11	0.94 ± 0.30	1.92 ± 0.66	8(40%)

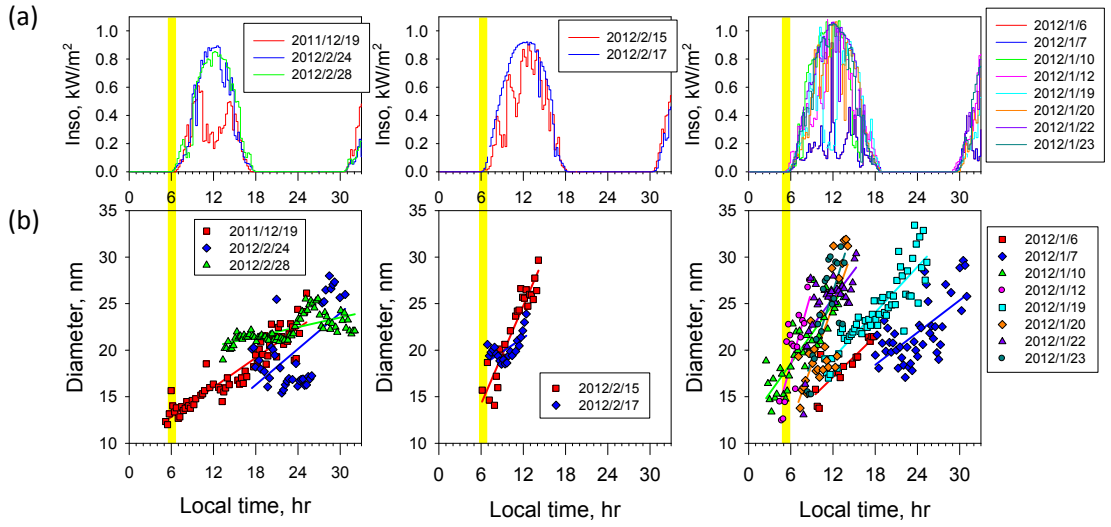

Fig. 11. Local-time temporal variation of solar irradiation and modal diameters of nucleation modes during NPF events. Lines of (b) represent linearization results for each event.

sunrise time (around 5 a.m. at local time) if the growth change was assumed to be a banana shape. The other two cases of NPF events (19 December 2011 and 12 January 2012) also started from before a few hours. These beginnings of the events were under easterly winds and easterly backward air mass trajectory conditions. Therefore, the air masses of those events might also have been transported after being affected by solar insolation.

Except for 15 and 28 February, the events were found under less-CS conditions (less than 1×10^{-3} s^{-1} at dry particle and less than 2×10^{-3} s^{-1} at ambient conditions) during daytime (Fig. 10 and Tables 5 and 6). The CS is the scavenging speed of gaseous molecules caused by condensation onto particles. Therefore, lower values denote conditions that are more favorable for NPF. For most events (9 events), less CS often corresponded with observed precipitation or cumulative precipitation (19 December 2011 and 24 February 2012 of NSP, 15 February 2012 of TP, 6, 7, 10, 12, 19, and 20 January 2012 of SSP in Fig. 10c and e). The less-CS resulted from less accumulation mode particles (Fig. 10), thereby implying a relation of in-cloud scavenging processing, as described in section 3.3. Some reports have described nucleation above MBL. Based on aircraft observations, nucleation events were observed in outflow regions of convective clouds in the tropics and mid-latitudes over the tropical area (Clarke et al., 1998a, b, 1999). In addition, transport attributable to subsidence and entrainment from the free troposphere into MBL for small particles was observed in the convective region (Bates et al., 1998; Clarke and Porter, 1993; Covert et al., 1996). In this study, the less-CS corresponded with precipitation. Although that implies in-cloud and below-cloud scavenging, the possibility also exists that the clean air derives from localized subsidence and entrainment enhanced around convective clouds. According to observation studies conducted at Christmas Island by Clarke et al. (1996), subsidence/convection was evaluated using diurnal variation of ozone concentration. Unfortunately, the ozone concentration in our study cannot be assessed similarly because our observation site was not fixed. However, if the less-CS condition resulted from subsidence, and O_3 was of a higher concentration at a higher altitude, the O_3 concentration can increase concomitantly with decreased CS. Based on temporal variation of O_3 concentration and CS in Fig. 10, no clear relation between them was found except for events of 19 December 2011 in NNP and 17 February 2012 in TP. The O_3 concentration during NPF events in Fig. 10 presents the average level of the area (Table 4). In addition, according to backward trajectories, vertical movements of air mass within a day were within 300 m, except 17 February 2012. These results were unsupportive of subsidence during NPF event, implying some probability. In this study, the possibility remains that occurrences of most NPF events and less-CS conditions in this study, especially over SSP, were originated in MBL.

The growth rates (GR in Tables 5 and 6) of nucleation mode particles for the NPF event (from appearance of nucleation mode to 30 nm) were obtained from the slope of the modal diameter of the nucleation mode by lognormal fitting of the number–size distribution for each 3 min. The growth rate and maximum number concentration of nucleation mode particles were estimated as

0.2–2.7 nm h^{-1} and 17–241 cm^{-3} (Tables 5 and 6). According to a review of studies for NPF events by Kulmala et al. (2004), typical particle growth rates were 1–20 nm h^{-1} at mid-latitudes depending on the temperature and availability of condensable vapors. Although reports of detailed analysis of NPF events over remote ocean areas are few, several reports have described growth during NPF in maritime environments. The growth rate for remote Pacific Ocean in this study tended to be somewhat lower than the growth rate (1.8–8.2 nm h^{-1}) of nucleation observed at remote coastal sites in sub-tropical Australia (Modini et al., 2009), the average values (2.7 nm h^{-1}) at marine areas near the coast of western Ireland (Ehn et al., 2010), and the values (0.8–3.6 nm h^{-1}) in marine boundary layer over the central Arctic Ocean (Karl et al., 2012). Current observed growth rates are in ranges among these observed rates over marine environments.

The typical average values of number concentration of nucleation mode during an NPF event (N_{nuclei} in Tables 5 and 6) in this study were 20–90 cm^{-3}, except for the event of 17 February 2012. The N_{nuclei} show comparable number concentrations to those of Aitken mode of NSP, TP2, and SSP1, but they are unlikely to be sufficient as a supply source to a high number concentration of Aitken mode particles in TP1 and SSP2. Although the NPF event of high number concentrations were unfortunately not observed around the SSP2 area, the N_{nuclei} of 17 February 2012 was high (241 cm^{-3}), comparable with the number concentration of the Aitken mode of TP1. Based on the backward air mass trajectory, the air mass in the case was derived from the upper altitude without precipitation. In addition, Fig. 10f shows that an increase of O_3 was found. Therefore, the NPF event was regarded as having been induced by a supply of a clean air mass from transport of upper boundary layer and not by precipitation. In the upper troposphere (8–12 km) over the tropical Pacific Ocean, high concentrations (5000–20,000 cm^{-3} STP) of newly formed aerosol particles smaller than 10 nm were observed frequently (Clarke and Kapustin, 2002). Higher concentrations of the Aitken mode of TP1 in this study might also be attributed to an air mass originating from higher altitudes.

According to previous studies, evidence of the nucleation in MBL probably does not exist (Bates et al., 1998; Quinn and Bates, 2011). Bates et al. (1998) have described that the presence of ultra-fine mode particles in the MBL is explainable by convective mixing between the free troposphere and the MBL associated with cloud pumping and subsidence following cold frontal passages. In this study, some NPF events were observed by ship observations, although the concentrations of nucleation mode were not high. Especially, for frequent NPF events at SSP, observed trace gas concentrations and backward air mass trajectory analyses did not contradict the possibility of occurrence in MBL of the NPF events. As explained in section 3.3, particles in the TP area were large and aged well, which caused high values of condensation sinks. In addition, the frequency and intensity of precipitation along the trajectories of southern hemisphere were less, but most NPF events were found with precipitation events. In contrast, CS in SSP2 was low because of weak precipitation. Certain gaseous DMS also existed (Table 7). DMS is the precursor gas of particulate matter (methanesulfonic acid) and SO_2 gases, which is a precursor gas of sulfate, and which originates from marine biological activity. The occurrence of NPF event over SSP might occur by the coincidental occurrence of both less-CS and the presence of precursor gas.

4. Summary and conclusions

Number–size distributions of aerosols of 10–500 nm diameter were observed over the Pacific Ocean during December 2011–March 2012. The obtained number–size distributions were analyzed to ascertain their relation with the condensation sink of precursor gases, air mass transport, meteorological conditions, chlorophyll concentrations along the trajectory, and DMS concentrations of atmosphere and seawater. Bimodal size distributions with mode peaks in 30–80 nm (Aitken mode) and 100–200 nm (accumulation mode) were observed frequently. Number concentrations and modal diameters of Aitken and accumulation modes in the northern Pacific, which has highly intense and frequent precipitation, were less than in other regions. Large modes were observed over the eastern equator. The 5-day backward trajectory shows that the air masses at the equator originate from a boundary layer over the high chlorophyll area without experiencing precipitation. These results suggest that the particles at the equator were able to age well without removal by precipitation.

New particle formation events were often observed over mid-latitudes in the eastern South Pacific, in accordance with the low concentration of accumulation mode particles. Most NPF events were found under low-CS conditions (less than 1×10^{-3} s^{-1} at dry condition) during daytime. Low CS often corresponded to observed precipitation or cumulative precipitation. Therefore, it is attributed to precipitation scavenging. The air mass was attributed to the marine boundary layer based on ozone concentration. In these observations, no new particle formation event was observed over the eastern equatorial area, an eutrophic sea area. Condensation of precursor gases onto pre-existing particles strongly inhibits the nucleation of fresh particles. Such condensation to pre-existing particles was sufficiently effective at the equator under non-precipitating conditions. Therefore, new particle formation would not be observed over the equator.

As discussed above, the number–size distribution and the NPF event frequency were characteristic, according to different sea areas and their conditions, particularly meteorological conditions along the air mass trajectory. In addition to effects of transport from the upper troposphere and continental area, our results suggest that precipitation and emission from marine biological productivity controlled the balances of formation and growth of aerosol particles, characterizing the horizontal variation of the number–size distribution.

Acknowledgments

We thank the crew of R/V *Hakuho maru* during KH-11-10 and KH-12-1 cruises for their kind assistance with our shipboard observations. We gratefully acknowledge the NOAA Air Research Laboratory (ARL) for provision of the HYSPLIT transport and dispersion model. This study was partly supported by a Grant-in-Aid for Scientific Research, Category C (Grant No. 22510019) from JSPS, supported by Steel Foundation for Environmental Protection Technology, and supported by the Sasakawa Scientific Research Grant from The Japan Science Society. Data related to this paper can be distributed by contacting the corresponding author, S. Ueda (ueda-s@stelab.nagoya-u.ac.jp).

References

Andreae, M.O., Elbert, W., Mora, S.J., 1995. Biogenic sulfur emissions and aerosols over the tropical South Atlantic 3, Atmospheric dimethylsulfide, aerosols and cloud condensation nuclei. J. Geophys. Res. 100 (D6), 11335–11356.

Andronache, C., 2004. Estimates of sulfate aerosol wet scavenging coefficient for locations in the Eastern United States. Atmos. Environ. 38, 795–804.

Bates, T.S., Coffman, D.J., Covert, D.S., Quinn, P.K., 2002. Regional marine boundary layer aerosol size distributions in the Indian, Atlantic, and Pacific Oceans: a comparison of INDOEX measurements with ACE-1, ACE-2, and Aerosols99. J. Geophys. Res. 107 (D19), 8026. http://dx.doi.org/10.1029/2001JD001174.

Bates, T.S., Kapustin, V.N., Quinn, P.K., Covert, D.S., Coffman, D.J., Mari, C., Durkee, P.A., Bruyn, W.J.D., Saltzman, E.S., 1998. Processes controlling the distribution of aerosol particles in the lower marine boundary layer during the first aerosol characterization experiment (ACE 1). J. Geophys. Res. 103 (D13),

16369–16383.
Charlson, R.J., Lovelock, J.E., Andreae, M.O., Warren, S.G., 1987. Oceanic phytoplankton, atmospheric sulfur, cloud albedo and climate. Nature 326, 655–661.
Clarke, A.D., Ahlquist, N.C., Covert, D.S., 1987. The Pacific marine aerosol: evidence for natural acid sulfates. J. Geophys. Res. 92 (D4), 4179–4190.
Clarke, A.D., Davis, D., Kapustin, V.N., Eisele, F., Chen, G., Paluch, I., Lenschow, D., Bandy, A.R., Thornton, D., Moore, K., Mauldin, L., Tanner, D., Litchy, M., Carroll, M.A., Collins, J., Albercook, G., 1998a. Particle nucleation in the tropical boundary layer and its coupling to marine sulfur sources. Science 282, 89–92. http://dx.doi.org/10.1126/science.282.5386.89.
Clarke, A.D., Kapustin, V.N., 2002. A Pacific aerosol survey: Part I. The decade of data on particle production, transport, evolution, and mixing in the troposphere. J. Atmos. Sci. 59, 363–382.
Clarke, A.D., Kapustin, V.N., Eisele, F.L., Weber, R.J., McMurry, P.H., 1999. Particle production near marine clouds: sulfuric acid and prediction from classical binary nucleation. J. Geophys. Res. 26 (D16), 2425–2428.
Clarke, A.D., Li, Z., Litchy, M., 1996. Aerosol dynamics in the equatorial Pacific Marine boundary layer: microphysics, diurnal cycles and entrainment. Geophys. Res. Lett. 23, 733–736.
Clarke, A.D., Owens, S.R., Zhou, J., 2006. An ultrafine sea-salt flux from breaking waves: implications for cloud condensation nuclei in the remote marine atmosphere. J. Geophys. Res. 111, D06202. http://dx.doi.org/10.1029/2005JD006565.
Clarke, A.D., Porter, J.N., 1993. Pacific marine aerosol 2. Equatorial gradients in chlorophyll, ammonium, and excess sulfate during SAGA 3. J. Geophys. Res. 98 (D9), 16997–17010.
Clarke, A.D., Varner, J.L., Eisele, F., Mauldin, R.L., Tanner, D., Litchy, M., 1998b. Particle production in the remote marine atmosphere: cloud outflow and subsidence during ACE 1. J. Geophys. Res. 103 (D13), 16397–16,409.
Covert, D.S., Kapustin, V.N., Bates, T.S., Quinn, P.K., 1996. Physical properties of marine boundary layer aerosol particles of the mid-Pacific in relation to sources and meteorological transport. J. Geophys. Res. 101 (D3), 6919–6930.
Covert, D.S., Kapustin, V.N., Quinn, P.K., Bates, T.S., 1992. New Particle Formation in the marine boundary layer. J. Geophys. Res. 97 (D18), 20581–20589.
Cox, R.A., Sandalls, F.J., 1974. The photo-oxidation of hydrogen sulphide and dimethyl sulphide in air. Atmos. Environ 8, 1269–1281.
Dal Maso, M., Kulmala, M., Riipinen, I., Wagner, R., Hussein, T., Aalto, P.P., Lehtinen, K.E.J., 2005. Formation and growth of fresh atmospheric aerosols: eight years of aerosol size distribution data from SMEAR II, Hyytiälä, Finland. Boreal Environ. Res. 10, 323–336.
Draxler, R.R., Rolph, G.D., 2003. HYSPLIT (HYbrid Single-particle Lagrangian Integrated Trajectory) Model Access via NOAA ARL READY. NOAA Air Resources Laboratory, Silver Spring, MD. Website. http://www.arl.noaa.gov/ready/hysplit4.html.
Dusek, U., Frank, G.P., Hildebrandt, L., Curtius, J., Schneider, J., Walter, S., Chand, D., Drewnick, F., Hings, S., Jung, D., Borrmann, S., Andreae, M.O., 2006. Size matters more than chemistry for cloud-nucleating ability of aerosol particles. Science 312, 1375–1378. http://dx.doi.org/10.1126/science.1125261.
Ehn, M., Vuollekoski, H., Petäjä, T., Kerminen, V.-M., Vana, M., Aalto, P., Leeuw, G., Ceburnis, D., Dupuy, R., O'Dowd, C.D., Kulmala, M., 2010. Growth rates during coastal and marine new particle formation in western Ireland. J. Geophys. Res. 115, D18218. http://dx.doi.org/10.1029/2010JD014292.
Eleftheriadisa, K., Colbeckb, I., Housiadasa, C., Lazaridisc, M., Mihalopoulosd, N., Mitsakoua, C., Smolíke, J., Ždímal, V., 2006. Size distribution, composition and origin of the submicron aerosol in the marine boundary layer during the eastern Mediterranean "SUB-AERO" experiment. Atmos. Environ. 40, 6245–6260.
Fitzgerald, J.W., 1973. Dependence 488 of the supersaturation spectrum of CCN on aerosol size distribution and composition. J. Atmos. Sci. 30, 628–634.
Fitzgerald, J.W., 1991. Marine aerosols: a review. Atmos. Environ. 25, 533–545.
Fuchs, N.A., 1964. The coagulation of aerosols. In: The Mechanics of Aerosols. Dover Publications, Inc., New York, pp. 288–322.
Fuchs, N.A., Sutugin, A.G., 1971. High-dispersed aerosols. In: Hidy, G.M., Brock, J.R. (Eds.), Topics in Current Aerosol Research. Pergamon, New York, pp. 1–60.
Gong, S.L., 2003. A parameterization of sea-salt aerosol source function for sub- and super-micron particles. Glob. Biogeochem. Cycles 17 (4), 1097. http://dx.doi.org/10.1029/2003GB002079.
Hanson, D.R., Eisele, F., 2000. Diffusion of H_2SO_4 in humidified nitrogen: hydrated H_2SO_4. J. Phys. Chem. A 104, 1715–1719.
Heintzenberg, J., Covert, D.C., Van Dingenen, R., 2000. Size distribution and chemical composition of marine aerosols: a compilation and review. Tellus B 52, 1104–1122.
Hoell, C., O'Dowd, C.D., Osborne, S.R., Johnson, D.W., 2000. Timescale analysis of marine boundary layer aerosol evolution: Lagrangian case studies under clean and polluted cloudy conditions. Tellus B 52, 423–438.
Hoppel, W.A., Frick, G.M., 1990. Submicron aerosol size distributions measured over the tropical and south Pacific. Atmos. Environ. 24A, 645–659.
Hoppel, W.A., Frick, G.M., Fitzgerald, J.W., 1994b. A cloud chamber study of the effect that nonprecipitating water clouds have on the aerosol size distribution. Aerosol Sci. Technol. 20, 1–30.
Hoppel, W.A., Frick, G.M., Fitzgerald, J.W., Larson, R.E., 1994a. Marine boundary layer measurements of new particle formation and the effects nonprecipitating clouds have on aerosol size distribution. J. Geophys. Res. D99 (14), 443–459.
Hoppel, W.A., Frick, G.M., Larson, R.E., 1986. Effect of nonprecipitating clouds on the aerosol size distribution in the marine boundary layer. Geophys. Res. Lett. 13, 125–128.
Husar, R.B., Whitby, K.T., 1973. Growth Mechanisms and size spectra of photochemical aerosols. Environ. Sci. Technol. 7, 241–247.
Iida, K., Stolzenburg, M.R., McMurry, P.H., Smith, J.N., 2008. Estimating nanoparticle growth rates from sizedependent charged fractions: analysis of new particle formation events in Mexico City. J. Geophys. Res. 113, D05207. http://dx.doi.org/10.1029/2007JD009260.
Inomata, S., Tanimoto, H., Kameyama, S., Tsunogai, U., Irie, H., Kanaya, Y., Wang, Z., 2008. Technical Note: determination of formaldehyde mixing ratios in air with PTR-MS: laboratory experiments and field measurements. Atmos. Chem. Phys. 8, 273–284.
Junge, C., McLaren, E., 1971. Relationship of cloud nuclei spectra to aerosol size distribution and composition. J. Atmos. Sci. 28, 382–390.
Kameyama, S., Tanimoto, H., Inomata, S., Tsunogai, U., Ooki, A., Takeda, S., Obata, H., Tsuda, A., Uematsu, M., 2010. High-resolution measurement of multiple volatile organic compounds dissolved in seawater using equilibrator inlet-proton transfer reaction-mass spectrometry (EI-PTR-MS). Mar. Chem. 122, 59–73. http://dx.doi.org/10.1016/j.marchem.2010.08.003.
Kameyama, S., Tanimoto, H., Inomata, S., Tsunogai, U., Ooki, A., Yokouchi, Y., Takeda, S., Obata, H., Uematsu, M., 2009. Equilibrator inlet – proton transfer reaction – mass spectrometry (EI-PTR-MS) for sensitive, high-resolution measurement of dimethyl sulfide dissolved in seawater. Anal. Chem. 81 (21), 9021–9026. http://dx.doi.org/10.1021/ac901630h.
Karl, M., Leck, C., Gross, A., Pirjola, L., 2012. A study of new particle formation in the marine boundary layer over the central Arctic Ocean using a flexible multicomponent aerosol dynamic model. Tellus 64 B 17158. http://dx.doi.org/10.13402/tellusb.v17164i17150.17158.
Kerminen, V.-M., Lihavainen, H., Komppula, M., Viisanen, Y., Kulmala, M., 2005. Direct observational evidence linking atmospheric aerosol formation and cloud droplet activation. Geophys. Res. Lett. 32 (L14803) http://dx.doi.org/10.1029/2005GL023130.
Köhler, H., 1936. The nucleus in and the growth of hygroscopic droplets. Trans. Faraday Soc. 32, 1152–1161.
Kulmala, M., Dal Maso, M., Mäkelä, J.M., Pirjola, L., Väkevä, M., Aalto, P., Miikkulainen, P., Hämeri, K., O'Dowd, C.D., 2001. On the formation, growth and composition of nucleation mode particles. Tellus B 53, 479–490.
Kulmala, M., Vehkamaki, H., Petaja, T., Dal Maso, M., Lauri, A., Kerminen, V.-M., Birmili, W., McMurry, P.H., 2004. Formation and growth rates of ultrafine atmospheric particles: a review of observations. J. Aerosol Sci. 35, 143–176.
Lewis, E.R., Schwartz, S.E., 2004. Sea Salt Aerosol Production. Mechanisms, Methods, Measurements, and Models. American Geophysical Union, Washington, DC.
Lihavainen, H., Kerminen, V.-M., Komppula, M., Hatakka, J., Aaltonen, V., Kulmala, M., Viisanen, Y., 2003. Production of "potential" cloud condensation nuclei associated with atmospheric new-particle formation in northern Finland. J. Geophys. Res. 108 (D24), 4782. http://dx.doi.org/10.1029/2003JD003887.
Lovelock, J.E., Maggs, R.J., Rasmussen, R.A., 1972. Atmospheric dimethyl sulphide and the natural sulphur cycle. Nature 237, 452–453, 1972.
Mamane, Y., Gottlieb, J., 1989. The study of heterogeneous reactions of carbonaceous particles with sulfur and nitrogen oxides using a single particles. J. Aerosol. Sci. 20, 575–584.
Meng, Z., Seinfeld, J.H., 1994. On the source of submicrometer droplet mode of urban and regional aerosols. Aerosol Sci. Technol. 20, 253–265.
Mochida, M., Nishita-Hara, C., Furutani, H., Miyazaki, Y., Jung, J., Kawamura, K., Uematsu, M., 2011. Hygroscopicity and cloud condensation nucleus activity of marine aerosol particles over the western North Pacific. J. Geophys. Res. 116, D06204. http://dx.doi.org/10.1029/2005JD006661.
Modini, R.L., Ristovski, Z.D., Johnson, G.R., He, C., Surawski, N., Morawska, L., Suni, T., Kulmala, M., 2009. New particle formation and growth at a remote, sub-tropical coastal location. Atmos. Chem. Phys. 9, 7607–7621.
Nishita, C., Osada, K., Kido, M., Matsunaga, K., Iwasaka, Y., 2008. Nucleation mode particles in upslope valley winds at Mount Norikura, Japan: implications for the vertical extent of new particle formation events in the lower troposphere. J. Geophys. Res. 113, D06202. http://dx.doi.org/10.1029/2007JD009302.
Nishita, C., Osada, K., Matsunaga, K., Iwasaka, Y., 2007. Number–size distributions of free tropospheric aerosol particles at Mt. Norikura, Japan: effects of precipitation and air mass transportation pathways. J. Geophys. Res. 112, D10213. http://dx.doi.org/10.1029/2006JD007969.
O'Dowd, C.D., Leeuw, G., 2007. Marine aerosol production: a review of the current knowledge. Phi. Trans. R. Soc. 365. http://dx.doi.org/10.1098/rsta.2007.2043.
Omori, Y., Tanimoto, H., Inomata, S., Kameyama, S., Takao, S., Suzuki, K., 2013. Evaluation of using unfiltered seawater for underway measurement of dimethyl sulfide in the ocean by online mass spectrometry. Limnol. Oceanogr. Methods 11, 549–560.
Pant, V., Deshpande, C.G., Kamra, A.K., 2009. The concentration and number–size distribution measurements of the Marine Boundary Layer aerosols over the Indian Ocean. Atmos. Res. 92, 381–393.
Quinn, P.K., Bates, T.S., 2011. The case against climate regulation via oceanic phytoplankton sulphur emissions. Nature 480, 51–56.
Raemdonck, H., Maenhaut, W., Andreae, M.O., 1986. Chemistry of marine aerosol over the tropical and equatorial Pacific. J. Geophys. Res. 91 (D8), 8623–8636.
Raes, F., Van Dingenen, R., Vignati, E., Wilson, J., Putaud, J.-P., Seinfeld, J.H., Adams, P., 2000. Formation and cycling of aerosols in the global troposphere. Atmos. Environ. 34, 4215–4240.
Roberts, G., Mauger, G., Hadley, O., Ramanathan, V., 2006. North American and Asian aerosols over the eastern Pacific Ocean and their role in regulating cloud

condensation nuclei. J. Geophys. Res. 111, D13205. http://dx.doi.org/10.1029/2005JD006661.
Rolph, G.D., 2003. Real-time Environment Applications and Display System (READY). NOAA Air Resour. Lab., Silver Spring, MD. Available at: http://www.arl.noaa.gov/ready/hysplit4.html.
Scott, B.C., 1982. Theoretical estimates of the scavenging coefficient for soluble aerosol particles as a function of precipitation type, rate and altitude. Atmos. Environ. 16, 1753–1762.
Seinfeld, J.H., Pandis, S.N., 2006. Atmospheric Chemistry and Physics, from Air Pollution to Climate Change, second ed. John Wiley and Sons, Inc., New York. 1203 pp.
Twomey, S., 1977. Atmospheric Aerosols, Developments in Atmospheric Science, 7. Elsevier, New York, 302 pp.
Twomey, S., Warner, J., 1967. Comparison of measurements of cloud droplets and cloud nuclei. J. Atmos. Sci. 24, 702–703.
Ueda, S., Hirose, Y., Miura, K., Okochi, H., 2014. Individual aerosol particles in and below clouds along a Mt. Fuji slope: modification of sea-salt-containing particles by in-cloud processing. Atmos. Res. 137, 216–227.
Vaattovaara, P., Huttunen, P.E., Yoon, Y.J., Joutsensaari, J., Lehtinen, K.E.J., O'Dowd, C.D., Laaksonen, A., 2006. The composition of nucleation and Aitken modes particles during coastal nucleation events: evidence for marine secondary organic contribution. Atmos. Chem. Phys. 6, 4601–4616.
Venzac, H., Sellegri, K., Laj, P., Villani, P., Bonasoni, P., Marinoni, A., Cristofanelli, P., Calzolari, F., Fuzzi, S., Decesari, S., Facchini, M.-C., Vuillermoz, E., Verza, G.P., 2008. High frequency new particle formation in the Himalayas. Proc. Natl. Acad. Sci. U.S.A. 105 (41), 15,666–15,671.
Whitby, K.T., 1978. The physical characteristics of sulfur aerosols. Atmos. Environ. 12, 135–159.